performance. The gain is 15 ± 1.5 dB in the frequency from 27.7 GHz to 28.7 GHz. The noise figure is 9 ± 1.5 dB.

V. Conclusion

A FET mount design method is established for 30-GHz-band low-noise amplifiers. Two design examples were shown using this method. One is 13-dB gain and 8.5-dB noise figure, the other is 15-dB gain and 9-dB noise figure.

Acknowledgment

The author wishes to thank Dr. K. Kondo, Mr. H. Kato, and Dr. H. Tohyama of the Yokosuka Electrical Communication Laboratory, N.T.T., for their valuable guidance and discussions.

References

[1] H. Tohyama and H. Mizuno, "23 GHz band GaAs MESFET reflection-type amplifier," *IEEE Trans. Microwave Theory Tech.*, vol. MTT-27, pp. 408–411, May 1979.
[2] M. Tanaka *et al.*, "GaAs FET amplifiers for use in communication satellite transponder," presented at the 31st Int. Astronautical Federation, Tokyo, Japan, Sept. 1980.
[3] H. Yamasaki *et al.*, "High performance low noise FET's operating from *X*-band through *Ka*-band," in *IEEE Int. Electron Devices Meeting Dig.*, pp. 106–109, 1980.
[4] C. F. Krumm, H. T. Suyematsu, and B. L. Walsh, "A 30-GHz GaAs FET amplifier," in *IEEE MTT-S Int. Microwave Symp. Dig.*, pp. 383–385, 1978.
[5] C. T. Li, P. T. Chen, and P. H. Wang, "A *K*-band ion implanted GaAsFET," in *Proc. European Microwave Conf.*, pp. 396–400, 1978.
[6] T. Itoh, "A method for analyzing shielded microstrip lines," *IECE(B)*, vol. 58-B, no. 1, pp. 24–29, 1975.
[7] C. A. Liechti, "Microwave field-effect transistor—1976," *IEEE Trans. Microwave Theory Tech.*, vol. MTT-24, pp. 279–300, June 1976.
[8] G. E. Brehm and G. D. Vendelin, "Biasing FET's for optimum performance," *Microwaves*, pp. 38–44, Feb. 1974.

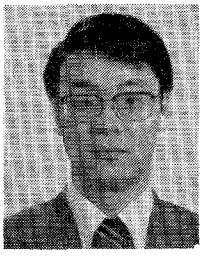

Hideki Mizuno was born in Niigata, Japan, on February 1, in 1952. He received the B.S. degree in electrical engineering from Tohoku University, Sendai, Japan, in 1975.

He joined the Yokosuka Electrical Communication Laboratory, Nippon Telegraph and Telephone Public Corporation, Yokosuka-shi, Kanagawa-ken, Japan, in 1975, and has since been engaged in research work on GaAsFET amplifiers for satellite communication systems. He is currently an Engineer of the Satellite Communication Equipment Section, Integrated Transmission System Development Division, Yokosuka Electrical Communication Laboratory.

Mr. Mizuno is a member of the Institute of Electronics and Communication Engineers of Japan.

Analysis of Image Recovery Down Converter Made by Planar Circuit Mounted in a Waveguide

YOZO UTSUMI, MEMBER, IEEE

Abstract—**This paper presents an analysis of a superhigh frequency (SHF) down converter using a Schottky-barrier mixer diode and a planar circuit mounted in a waveguide. The analysis assumes that the mixer diode consists of a nonlinear conductance g, a junction capacitance C_j, an ohmic spreading resistance R_s, and several parasitic susceptances. The frequency performance of the impedance of external circuits at the signal, image, and intermediate frequency bands is considered.**

This analysis also includes consideration of the mismatching effect between the converter and the IF amplifier, and the optimum design procedure for the down converter.

Using this theoretical method, a SHF down converter was designed and constructed. Its application is low-noise receivers for satellite broadcasting. The design used the optimum image condition (the image impedance takes a low value, i.e., nearly a short). The RF band is 11.7–12.2 GHz, the IF band is 0.96–1.46 GHz, and the total noise figure is 3.3–3.7 dB. The noise figure is in good agreement with the value (3.2–3.6 dB) obtained from this analysis.

Manuscript received November 23, 1981; revised January 29, 1982.

The author is with Technical Research Laboratories of Nippon Hoso Kyokai, 1-10-11, Kinuta, Setagaya-ku, Tokyo 157, Japan.

Nomenclature

g	Schottky junction nonlinear conductance of mixer diode.
C_j	Schottky junction capacitance of mixer diode.
$g_0 g_p g_{2p}$	Fourier expanded components of g.

0018-9480/82/0600-0858$00.75 ©1982 IEEE

C_0, C_p, C_{2p} Fourier expanded components of C_j.

R_s Series ohmic spreading resistance of mixer diode.

C_c Case capacitance of mixer diode.

L Lead wire inductance plus convergence inductance of mixer diode (from electrode to lead wire).

$X_{Ls}(X_{Lm})$ Equivalent circuit element, series reactance for capacitive matching strip C at signal (image) frequency.

$B_{cs}(B_{cm})$ Equivalent circuit element, shunt susceptance for capacitive matching strip C at signal (image) frequency.

$X'_{Ls}(X'_{Lm})$ Equivalent circuit element, series reactance for open-ended ridged guide transformer T at signal (image) frequency.

$B'_{cs}(B'_{cm})$ Equivalent circuit element, shunt susceptance for open-ended ridged guide transformer T at signal (image) frequency.

$n_s(n_m)$ Equivalent circuit element, transformer ratio for open-ended ridged guide transformer T at signal (image) frequency.

L_s Equivalent circuit element, series inductance for IF matching circuit M.

n_i Equivalent circuit element, transformer ratio for IF matching circuit M.

L_W Coupling inductance expressing exponentially decayed IF component in waveguide.

Z_0 Characteristic impedance of waveguide.

X_m Backward image reactance at terminal m.

y'_m Intrinsic image admittance at terminal m'.

$Z_{Fs}(Z_{Fm})$ Backward impedance of X-band rejection filter R viewed from mixer diode at signal (image) frequency.

$\theta_{1s}(\theta_{1m}) \sim \theta_{3s}(\theta_{3m})$ (θ_{4m}) Electrical length of each transmission line at signal (image) frequency.

$Z_{1s}(Z_{1m}) \sim Z_{3s}(Z_{3m})$ (Z_{4m}) Characteristic impedance of each transmission line at signal (image) frequency.

$\theta_5 \sim \theta_7$ Electrical length of each arm of X-band rejection filter R at intermediate frequency.

$Z_5 \sim Z_7$ Characteristic impedance of each arm of X-band rejection filter R at intermediate frequency.

$y_{sx}, y''_{sx}, y_{ia}, y'_{ia}, y''_m$ Input admittance at terminal s, s', i, i', and m'.

$g'_{sa}, g'_{sx}, g'_{ia}$ Real part of y'_{sa}, y'_{sx}, and y'_{ia}.

$y_{sa}, y'_{sa}, y_{ia}, y'_{ia}$ Outward admittance viewed from terminal s, s', i, and i'.

$y'_{s1}, y'_{s2}, y'_{i1}, y'_{i2}, y''_{m1}, y''_{m2}$ Input admittance at terminal s'_1, s'_2, i'_1, i'_2, m'_1, and m'_2.

g'_{s1}, g''_{m1} Real part of y'_{s1} and y''_{m1}.

$y'_{s1l}, y'_{s2l}, y'_{i1l}, y'_{i2l}, y'_{m1}, y'_{m2}$ Outward admittance viewed from terminal s'_1, s'_2, i'_1, i'_2, m'_1, and m'_2.

g'_{i1l}, g'_{m1} Real part of y'_{i1l} and y'_{m1}.

V'_s, V'_i, V'_m Voltage at terminal s', i', and m'.

I'_s, I'_i, I'_m Current flowing into terminal s', i', and m'.

$I'_{s1}, I'_{s2}, I'_{i1}, I'_{i2}, I'_{m1}, I'_{m2}$ Current flowing into terminal s'_1, s'_2, i'_1, i'_2, m'_1 and m'_2.

L_c Conversion loss of superhigh frequency (SHF) down converter.

L'_c Conversion loss of semiconductor portion ($s' \sim i'$).

L_1 Transmission loss caused by R_s in signal circuit ($s \sim s'$).

L_2 Transmission loss caused by R_s in IF circuit ($i' \sim i$).

L_{sin} Mismatching loss at terminal s.

t Noise temperature ratio of diode mixer.

t_{a1} Noise temperature ratio corresponding to thermal noise generated at R_s in signal circuit.

t_{a2} Noise temperature ratio corresponding to thermal noise generated at R_s in IF circuit.

t_{am} Noise temperature ratio corresponding to thermal noise generated at R_s in image circuit.

t'_{ac} Noise temperature ratio corresponding to shot noise generated in g circuit.

F Noise figure of SHF down converter.

F_{if} Noise figure of IF preamplifier.

N_s, N_i, N_m Shot noise power supplied from g circuit to g'_{s1l}, g'_{i1l}, and g'_{m1}

I_{ns}, I_{ni}, I_{nm} Shot noise current supplied from g circuit to y'_{s1l}, y'_{i1l}, and y'_{m1}.

$I_{s1o}, I_{i1o}, I_{m1o}$ Output shot noise current at terminals s'_1, i'_1, and m'_1 of g circuit which originate from shot noise power N_i, N_s, and N_m.

$I_{s2o}, I_{i2o}, I_{m2o}$ Output shot noise current at terminal s'_2, i'_2, and m'_2 of C circuit which originate from shot noise power N_i, N_s, and N_m.

I_{io} Total output shot noise current at terminal i'.

L'_{gsi} Conversion loss ($s'_1 \rightarrow i'_1$) with loaded y'_{m1} at terminal m'_1.

L'_{gis} Conversion loss ($i'_1 \rightarrow s'_1$) with loaded y'_{m1} at terminal m'_1.

L'_{gsm} Conversion loss ($s'_1 \rightarrow m'_1$) with loaded y'_{i1l} at terminal i'_1.

L'_{gms} Conversion loss ($m'_1 \rightarrow s'_1$) with loaded y'_{i1l} at terminal i'_1.

L'_{gim} Conversion loss ($i'_1 \rightarrow m'_1$) with loaded y'_{s1l} at terminal s'_1.

L'_{gmi} Conversion loss ($m'_1 \rightarrow i'_1$) with loaded y'_{s1l} at terminal s'_1.

$L_{s1,in}$ Input mismatching loss at terminal s'_1.

$L_{i1,in}$ Input mismatching loss at terminal i'_1.

$L_{m1,in}$ Input mismatching loss at terminal m'_1.

$L_{s1,out}$ Output mismatching loss at terminal s'_1.

$L_{i1,out}$ Output mismatching loss at terminal i'_1.

$L_{m1,out}$ Output mismatching loss at terminal m'_1.

α, β Current transfer function.

I. Introduction

THE NEED for down converters is increasing, especially for low-noise receivers used for satellite broadcasting and several other kinds of Microwave receivers [1]–[5]. The basic principles of down converters were described in depth by Torrey and Whitmer [6]. Many kinds of analyses of down converters have been made with special image conditions such as short, open, or matching [2], [7]–[9]. Kim made an analysis [10] of the tunnel diode and obtained the conversion loss and the noise figure only considering the nonlinear conductance g.

A powerful method for analyzing the conversion loss and the noise of mixers was published in 1978 by Held and Kerr [11], [12]. Reference [11] shows the theoretical universal approach, which includes the effect of local oscillator wave forms, and harmonics, and considers arbitrary embedding impedances and effects of the junction capacitance.

In this paper, the principal interest exists in making a practical design of a low-noise SHF down converter made by a planar circuit mounted in a waveguide. Therefore the analyses of the frequency performance of external circuits and the mismatching effects at the IF port are emphasized. A simplified model where only the signal, IF, and image frequencies are considered, is used to get simple algebraic forms of equations expressing a clear physical image how the shot noise is generated and affected by the junction capacitance.

Analyses of the noise performance of a Schottky-barrier diode mixer have already been published considering arbitrarly image impedances and the effect of a junction capacitance C_j [4], [5], [13]–[16]. These analyses have made clear the following points.

1) Increasing the value of the image impedance, the shot noise of the IF component is amplified and converted to the signal and the image frequency component again by the effect of the parametric up-converter action of the junction capacitance C_j. This effect makes the value of the noise figure large, although it makes the value of the conversion loss small.

2) The image impedance satisfying the optimum design condition of the down converter is low, i.e., nearly a short-circuit.

However, these analyses have been limited to the Schottky-barrier mixer diode itself, and the frequency performance of external circuits or mismatching effects have not been included. These analyses are thus not sufficient to design an actual down converter.

Original points of the present paper are the following: 1) the frequency performance of the SHF down-converter noise figure is obtained theoretically; 2) in the noise analysis, the frequency performance of the impedance of external circuits at the signal, image, and intermediate frequency bands are included; 3) the mismatching effect between the mixer diode and the IF amplifier is considered; 4) the approximation where the IF frequency f_i is sufficiently small compared with the signal or image frequency f_s or f_m is not used, and the down converter action of C_j is considered also.

Therefore, it is possible to achieve an optimum design and minimum noise figure of the actual down converter by using this proposed theoretical method.

Finally, the experimental results of the low-noise down converter using a planar circuit mounted in a waveguide are shown compared with the theoretical results obtained by this analysis.

II. Construction of SHF Down Converter

We constructed a SHF down converter under the image short condition with a Schottky-barrier mixer diode and a planar circuit mounted in a waveguide.

The construction of this newly developed SHF down converter is shown in Fig. 1. In Fig. 1, the band rejection filter for the local oscillator's frequency is abridged because the value of the external Q of this filter is extremely high, and the filter has no effect at the signal or image frequency bands. D in the figure indicates a Schottkey-barrier mixer diode; L_m a band rejection filter for the image frequency band; C a capacitive matching strip for the signal frequency band; T an open-ended ridged guide transformer; P a bandpass filter for the local oscillator frequency; R a X-band rejection filter; M an IF matching circuit; A an IF preamplifier; and PCMW a planar circuit mounted in a waveguide. Additionally, θ_1–θ_7 and Z_1–Z_7 indicate the electrical length and the characteristic admittance of the each transmission line.

The functions of several external circuits mentioned

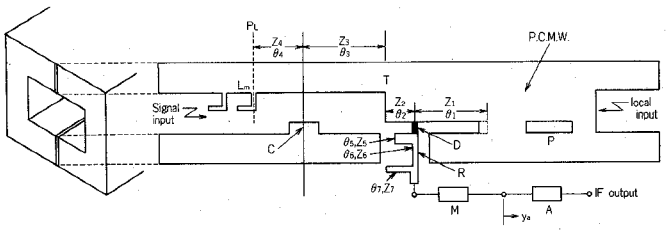

Fig. 1. Construction of SHF down converter.

above are explained more precisely in Section IV.

The equivalent circuit of the SHF down converter shown in Fig. 1 is obtained in the next section.

III. Equivalent Circuit and Noise Analysis of SHF Down Converter

A. Equivalent Circuit

The equivalent circuit of the SHF down converter with consideration of the frequency performance of the external circuits at the signal, image, and intermediate frequency bands is shown in Fig. 2(a). The semiconductor portion of a mixer diode takes an equivalent circuit [5], [13], [15] in which g and C_j are connected in parallel at terminal s', i', and m' as shown in Fig. 2(b). Many of the notations in Fig. 2 are found in the nomenclature.

This proposed analysis has been made considering all frequency performances at every port (signal, image, and IF) correlatively as shown in Fig. 2(a).

B. Noise Analysis

The relation between current and voltage of a mixer diode is expressed by (1). When the pumping voltage $V_0 + V_1 \cos\theta$ is impressed on the diode, g and C_j vary with $n \times f_p$ frequencies (n is an integer and f_p is a pumping frequency), and their Fourier expanded components are given by (2)

$$i = i_0(e^{\alpha v} - 1) \tag{1}$$

$$g_{np} = \alpha \cdot i_0 \cdot I_n(\alpha V_1)$$

$$C_{np} = \frac{C}{2\pi}\int_0^{2\pi} \frac{\cos n\theta}{\sqrt{1-(V_0+V_1\cos\theta)/V_\phi}}\,d\theta \tag{2}$$

where I_n is the modified Bessel function; C is the junction capacitance with zero bias voltage; V_ϕ is the junction voltage; α, i_0 is the proportional constant.

Using Fourier expanded components of g_{np}, C_{np} and the signal (ω_s), IF ($\omega_i = \omega_s - \omega_p$) and image ($\omega_m = 2\omega_p - \omega_s$) angular frequencies, the relation between each of the currents and voltages of Fig. 2(a) and (b) are expressed by (3), where the asterisk (*) indicates the complex conjugate

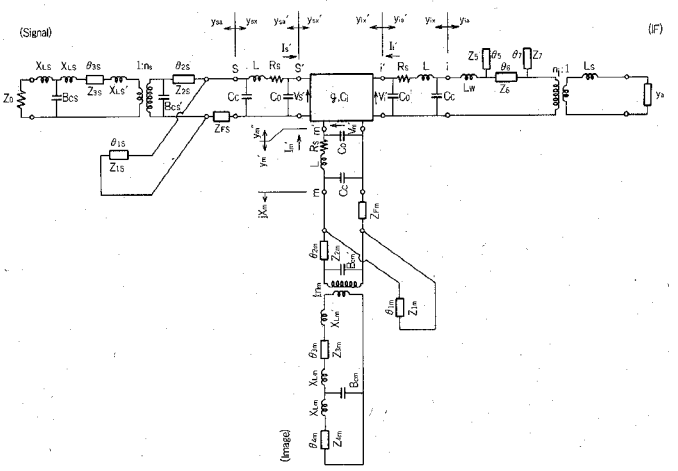

(a)

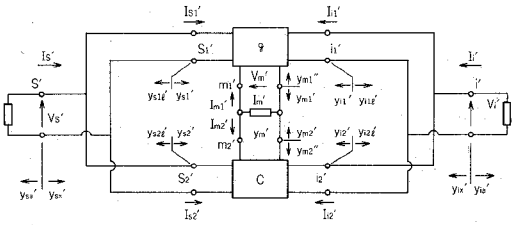

(b)

Fig. 2. Equivalent circuit of SHF down converter. (a) Equivalent circuit of SHF down converter. (b) Equivalent circuit of semiconductor's part of mixer diode.

Loading y'_m at terminal m' ($-I'_m = y'_m V'_m$), the relation shown in (4) can be obtained. y'_m is a function of the load reactance jX_m at terminal m as shown in (4). jX_m is expressed by several circuit parameters shown in Fig. 2(a)

$$\begin{bmatrix} I'_s \\ I'_i \end{bmatrix} = \begin{bmatrix} Y'_{ss} & Y'_{si} \\ Y'_{is} & Y'_{ii} \end{bmatrix} \cdot \begin{bmatrix} V'_s \\ V'_i \end{bmatrix}$$

$$Y'_{ss} = g_0 - \frac{(g_{2p} + j\omega_s C_{2p})(g_{2p} - j\omega_m C_{2p})}{g_0 + y'^*_m}$$

$$Y'_{si} = g_p + j\omega_s C_p - \frac{(g_{2p} + j\omega_s C_{2p})(g_{2p} - j\omega_m C_p)}{g_0 + y'^*_m}$$

$$Y'_{is} = g_p + j\omega_i C_p - \frac{(g_{2p} - j\omega_m C_{2p})(g_p + j\omega_i C_p)}{g_0 + y'^*_m}$$

$$Y'_{ii} = g_0 - \frac{(g_p + j\omega_i C_p)(g_p - j\omega_m C_p)}{g_0 + y'^*_m}$$

$$y'_m = j\omega_m C_0 + \frac{-j\cdot 1/X_m + j\omega_m C_c}{1 + (R_s + j\omega_m L)\cdot(-j\cdot 1/X_m + j\omega_m C_c)}$$

$$\begin{bmatrix} I'_s \\ I'_i \\ I'^*_m \end{bmatrix} = \begin{bmatrix} I'_{s1} \\ I'_{i1} \\ I'^*_{m1} \end{bmatrix} + \begin{bmatrix} I'_{s2} \\ I'_{i2} \\ I'^*_{m2} \end{bmatrix} = \begin{bmatrix} g_0 & g_p & g_{2p} \\ g_p & g_0 & g_p \\ g_{2p} & g_p & g_0 \end{bmatrix} \cdot \begin{bmatrix} V'_s \\ V'_i \\ V'^*_m \end{bmatrix} + \begin{bmatrix} 0 & j\omega_s C_p & j\omega_s C_{2p} \\ j\omega_i C_p & 0 & j\omega_i C_p \\ -j\omega_m C_{2p} & -j\omega_m C_p & 0 \end{bmatrix} \cdot \begin{bmatrix} V'_s \\ V'_i \\ V'^*_m \end{bmatrix}. \tag{3}$$

and

$$jX_m = Z_{Fm} + j\cdot 1/\left(\frac{1}{Z_{2m}}\cdot\frac{U_1\cdot\tan\theta_{2m}+Z_{2m}}{Z_{2m}\cdot\tan\theta_{2m}-U_1}+\frac{1}{Z_{1m}}\cot\theta_{1m}\right)$$

$$U_1 = 1/\left(B'_{cm}-\frac{1}{n_m^2 U_2}\right)$$

$$U_2 = X'_{Lm}+Z_{3m}\cdot\frac{U_3+Z_{3m}\cdot\tan\theta_{3m}}{Z_{3m}-U_3\cdot\tan\theta_{3m}}$$

$$U_3 = X_{Lm}-1/\left(B_{cm}-\frac{1}{X_{Lm}+Z_{4m}\cdot\tan\theta_{4m}}\right). \quad (4)$$

Using the mismatching load admittances y'_{sa} and y'_{ia} at terminal s' and i' in (4), (5) can be obtained

$$y'_{sx}=\frac{I'_s}{V'_s}=Y'_{ss}-\frac{Y'_{si}Y'_{is}}{Y'_{ii}+y'_{ia}} \qquad y'_{ix}=\frac{I'_i}{V'_i}=Y'_{ii}-\frac{Y'_{si}Y'_{is}}{Y'_{ss}+y'_{sa}}. \quad (5)$$

y'_{sa} and y'_{ia} in (5) can be expressed by (6) by using several circuit parameters shown in Fig. 2(a)

$$y'_{sa} = j\omega_s C_0 + 1/\left(R_s + j\omega_s L + \frac{1}{y_{sa}+j\omega_s C_c}\right)$$

$$y_{sa} = 1/\left\{Z_{Fs}+1/\left(\frac{1}{Z_{2s}}\cdot\frac{Z_{2s}+jV_1\cdot\tan\theta_{2s}}{V_1+jZ_{2s}\tan\theta_{2s}}-j\frac{1}{Z_{1s}}\cot\theta_{1s}\right)\right\}$$

$$V_1 = 1/\left(jB'_{cs}+\frac{1}{n_s^2 V_2}\right)$$

$$V_2 = jX'_{Ls}+Z_{3s}\cdot\frac{V_3+jZ_{3s}\cdot\tan\theta_{3s}}{Z_{3s}+jV_3\cdot\tan\theta_{3s}}$$

$$V_3 = jX_{Ls}+1/\left(jB_{cs}+\frac{1}{Z_0+jX_{Ls}}\right)$$

$$y'_{ia} = j\omega_i C_0 + 1/\left(R_s + j\omega_i L + \frac{1}{y_{ia}+j\omega_i C_c}\right)$$

$$y_{ia} = 1/\left\{j\omega_i L_W + 1/\left(\frac{1}{Z_6}\cdot\frac{Z_6+jW_1\cdot\tan\theta_6}{W_1+jZ_6\cdot\tan\theta_6}+j\frac{1}{Z_5}\tan\theta_5\right)\right\}$$

$$W_1 = 1/\left\{n_i^2\cdot\left(j\omega_i L_s+\frac{1}{y_a}\right)\right\}+j\frac{1}{Z_7}\tan\theta_7. \quad (6)$$

Many circuit parameters in (4) and (6) will be given in Sections IV and VI.

In the case of the conjugate matching at terminal s' and i' ($y'_{sa}=y'^{*}_{s}$, $y'_{ia}=y'^{*}_{i}$), analysis of the input and output matching admittances, the conversion loss, and the noise figure with consideration of arbitrary image impedances and the effects of C_j has already been accomplished [5], [15] at a fixed frequency (signal frequency, $f_s=12.075$ GHz; intermediate frequency, $f_i=380$ MHz). In this analysis [5], [15] the approximation of $\omega_i \ll \omega_s, \omega_m$ has been used, and the down-converter action of C circuit shown in Fig. 2(b) has been neglected.

The present paper describes the frequency performance of this down converter with consideration of the external

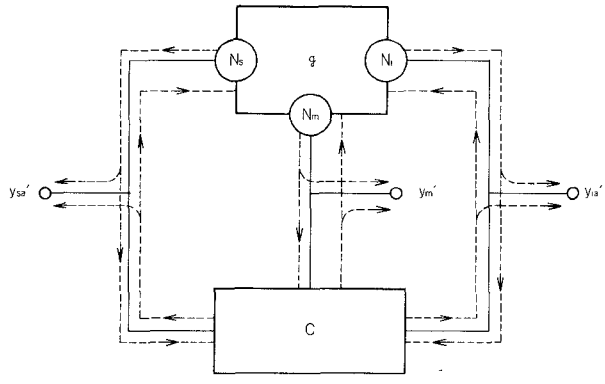

Fig. 3. Power flow of shot noise with considering down converter action of C_j

circuit frequency performance and the mismatching effect between the converter and the IF amplifier. In this analysis, the signal frequency band is 11.7–12.2 GHz and the IF band is 0.96–1.46 GHz. Therefore the approximation of $\omega_i \ll \omega_s, \omega_m$ cannot be used, and the down-converter action of C circuit cannot be neglected. The power flow of the shot noise is shown in Fig. 3. In Fig. 3, N_s is the shot noise power supplied to the outward admittance at the signal port of g circuit, N_i is that at the IF port, and N_m is that at the image port, respectively.

The conversion loss L_c between terminal s and i in Fig. 2(a) can be obtained as shown in (7) by using the relations of (3)–(6).

$$L_c = L_{\sin}\cdot L_1\cdot L'_c\cdot L_2$$

$$L_{\sin}=\frac{|y'_{sa}+y'_{sx}|^2}{4g'_{sa}\cdot g'_{sx}}$$

$$L_1 = 1+\frac{R_s\cdot|j\omega_s C_0+y'_{sx}|^2}{g'_{sx}}$$

$$L'_c=\frac{|Y'_{si}|^2}{|y'_{sx}-Y'_{ss}|^2}\cdot\frac{g'_{sx}}{g'_{ia}}$$

$$L_2 = 1+R_s\cdot\left|\frac{y'_{ia}-j\omega_i C_0}{1-R_s y'_{ia}+j\omega_i C_0 R_s}\right|^2 \Big/ \mathrm{Re}\left(\frac{y'_{ia}-j\omega_i C_0}{1-R_s y'_{ia}+j\omega_i C_0 R_s}\right) \quad (7)$$

where Re signifies the real part of the complex function. The values of y'_{sa}, y'_{sx}, and y'_{ia} can also be calculated by (5) and (6).

The concept of the noise temperature ratio is also useful for analyzing the noise performance of the SHF down converter. It is necessary to clarify the definition of the noise temperature ratio of the down converter. The noise power absorbed in the IF output load which is generated in the down converter itself, including the shot noise and the thermal noise, is defined as N_a. The maximum thermal noise power absorbed in the IF output load per 1 Hz is kT_0, where k is a Boltzman constant, and all circuits are

kept in $T_0[K]$. The noise temperature ratio t is then defined as shown in (8)

$$t = \frac{1}{L_c} + \frac{N_a}{kT_0}. \tag{8}$$

In order to consider the relation between conversion loss and noise performance, it is first necessary to obtain the noise-temperature ratio corresponding to the thermal noise generated at R_s in each terminal. The noise-temperature ratios corresponding to the thermal noise generated at R_s in a signal, IF and image circuit are defined as t_{a1}, t_{a2}, and t_{am}, respectively. The values of t_{a1} and t_{a2} can be obtained by (9) and (10), which are deduced from (8) and Fig. 2(a)

$$t_{a1} = \frac{1}{L_c' L_2}\left(1 - \frac{1}{L_1}\right) \tag{9}$$

$$t_{a2} = 1 - \frac{1}{L_2}. \tag{10}$$

The equivalent noise voltage per hertz induced by R_s which is kept in $T_0[K]$ at the image circuit is defined as $e_m (= \sqrt{4kT_0R_s})$. The noise voltage V_m' at terminal m' caused by e_m can be then obtained as shown in (11)

$$V_m' = \frac{y_m' - j\omega_m C_0}{y_m' + y_m''} \cdot \sqrt{4kT_0R_s}. \tag{11}$$

The relation between V_m' and V_t' is as shown in (12)

$$V_t' = A_{tm} V_m'^* \tag{12}$$

where A_{tm} is that given in (A4). Therefore t_{am} can be obtained as shown in (13) by using (11) and (12)

$$t_{am} = 4R_s \cdot \left|\frac{y_m' - j\omega_m C_0}{y_m' + y_m''}\right|^2 \cdot |A_{tm}|^2 \cdot g_t' \cdot \frac{1}{L_2}. \tag{13}$$

In (13), the value of y_m' must be calculated by (4), and y_m'' can be obtained by (14)

$$y_m'' = g_0 + (g_p + j\omega_m C_p) A_{tm}^* + (g_{2p} + j\omega_m C_{2p}) A_{sm}^* \tag{14}$$

where A_{sm} also is given by (A4).

Next it is necessary to obtain the shot noise generated in a g circuit of Fig. 2(b). Then the noise-temperature ratio t_{ac}' corresponding to the shot noise generated in the g circuit can be obtained as shown in (15), where B_t, B_s, and B_m are given by (A7), (A9), and (A10), and $A_1 - A_6$ can be obtained by (A13) and (A14), and $n = 19.5/\alpha$. The derivation of t_{ac}' is explained in detail in the Appendix

$$t_{ac}' = \frac{ng_{ta}'}{L_2}\left(\frac{|B_t| \cdot |y_{t1l}'|^2}{g_{t1l}'} \cdot \left|\frac{A_1}{y_{t1l}'} - \frac{A_2}{y_{t2l}'}\right|^2 + \frac{|B_s| \cdot |y_{s1l}'|^2}{g_{s1l}'} \cdot \left|\frac{A_3}{y_{t1l}'} - \frac{A_4}{y_{t2l}'}\right|^2 + \frac{|B_m| \cdot |y_{m1}'|^2}{g_{m1}'} \cdot \left|\frac{A_5}{y_{t1l}'} - \frac{A_6}{y_{t2l}'}\right|^2\right). \tag{15}$$

By using (7), (9), (10), (13), and (15), the total noise-temperature ratio t can be obtained as shown in (16)

$$t = \frac{1}{L_c} + t_{a1} + t_{a2} + t_{am} + t_{ac}'. \tag{16}$$

In the case of connecting a mismatched IF preamplifier at the IF port of the down converter, the total noise figure F can be expressed by (17), where L_c and t are given by (7) and (16), respectively, and the noise figure of the IF preamplifier F_{if} is given by Fig. 11, and $|\Gamma|$ is the absolute value of the reflection coefficient at the IF port

$$F = L_c\left(t + \frac{F_{if} - 1}{1 - |\Gamma|^2}\right). \tag{17}$$

IV. Frequency Performance of External Circuits

The frequency performance of the following external circuits must be obtained for the noise analysis described in Section III and the Appendix.

A. Capacitive Strip

The capacitive strip C and its equivalent circuit [17] are shown in Fig. 4. In Fig. 4, the solid line means the series inductive reactance X_L normalized by the input or output impedance. The dotted line is the shunt capacitive reactance $X_c (= -1/B_c)$.

This capacitive strip is useful for impedance matching in the signal frequency band by adjusting the value of S and its location in the waveguide.

B. Open-Ended Ridged Guide Transformer

The open-ended ridged guide transformer T and its equivalent circuit have been shown in [17, fig. 7]. In its figure X_L' signifies the series inductive reactance normalized by the input or output impedance, B_c' the shunt capacitive susceptance, and n the transformer ratio.

It is possible to select the proper value of n by adjusting the value of a gap S. The proper values of n and θ_{3s} then broaden the frequency characteristic of the noise figure.

C. Short-Ended Ridged Guide

The effective length l_{eff} between an arbitrary point P and the short-circuit point of the short-ended ridged guide is larger than the actual length l with the relation of (18) [17]

$$l_{\text{eff}} = l + \Delta l. \tag{18}$$

The measured values of Δl have been shown in [17, fig. 4]. The dotted line near the short-circuit point of the short-ended ridged guide in Fig. 1 corresponds to this length Δl.

In order to maintain optimum image conditions, the value of l_{eff} must be selected to be about a half-wavelength at the image frequency.

D. Image Rejection Filter

The image rejection filter L_m and its performance are shown in Fig. 5. In Fig. 5, the image suppression of this filter is greater than 32 dB at the frequency band used.

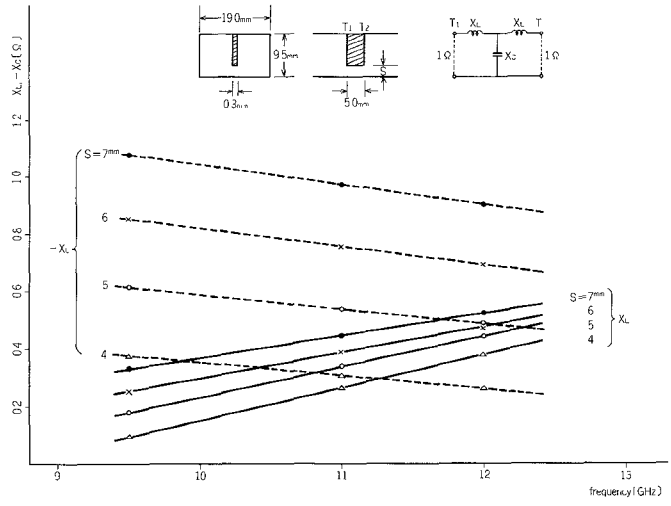

Fig. 4. Capacitive strip and its equivalent circuit.

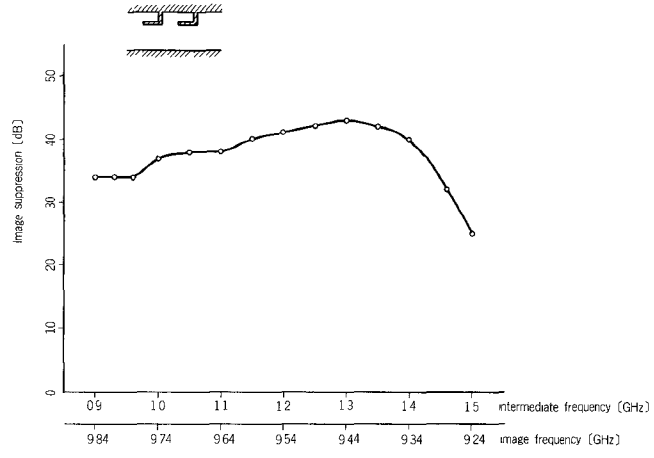

Fig. 5. Image suppression of image rejection filter.

And the total image suppression of the down converter including the effect of this filter and other external circuits is greater than 40 dB at this frequency band. The left ward impedance viewed from point P_L in Fig. 1 at the image frequency band is assumed short, as shown in Fig. 2(a). The VSWR of this filter at the signal frequency band is less than 1.1. Therefore it can be assumed that this filter has no effect approximately at the signal frequency band.

E. X-Band Rejection Filter

The X-band rejection triplate type filter R and its impedance characteristics are shown in Fig. 6. In Fig. 6, the solid line shows the measured value and the dotted line the theoretical value. The backward impedances Z_{Fs} and Z_{Fm} appeared in Fig. 2(a) can thus be obtained from this impedance characteristic.

This filter suppresses the power in the signal, image, and local frequencies by more than 25 dB, and passes only the IF power.

F. IF Coupling Inductance at Waveguide

The measured value of the coupling inductive impedance ωL_W expressing an exponentially decayed IF component in

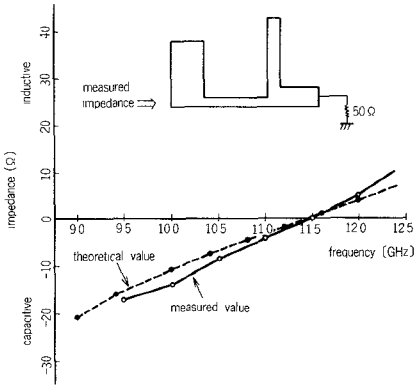

Fig. 6. X-band rejection triplate type filter and its impedance characteristic.

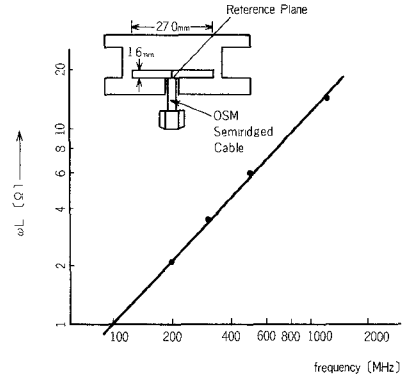

Fig. 7. IF coupling inductive impedance at waveguide.

a waveguide is shown in Fig. 7. The value of L_W can be obtained as approximately 1.8 nH.

V. Design of SHF Down Converter

In order to design the SHF down converter, several external circuits must be selected, first to make the image impedance low and capacitive. Secondly, the matching condition at terminal s when connecting a mismatched IF preamplifier at the IF port must be examined. Finally the noise analysis must be made considering the frequency performance of every external circuit. The outline of this design is described below.

A. Image Impedance

After adjusting several external circuits (θ_{1m} Z_{1m}, θ_{4m}, Z_{4m}, and Z_{Fm}) by using the results shown in Figs. 4, 5, and 6 and reference [17], the image impedance jX_m decided by the frequency performance of the external circuits can then be obtained by (4) as shown in Fig. 8. In Fig. 8, the value of the operating image reactance X_m is -36 to -13 Ω. The result shows operation at a low capacitive impedance near a short-circuit. The optimum image condition described in Section I can therefore be ensured. And then the normalized intrinsic image admittance $\bar{y}'_m$ is shown in Fig. 9. These values show low impedances almost near a short circuit, and the small real part is due to a series resistance R_s.

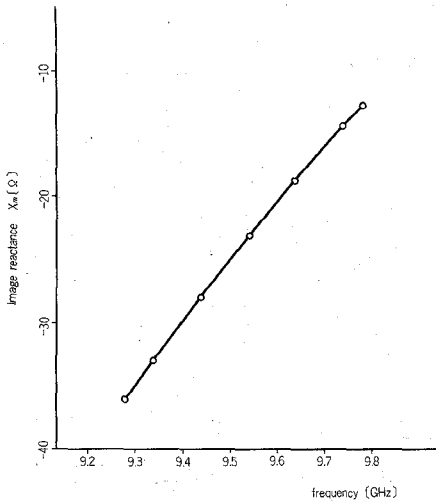

Fig. 8. Frequency performance of image impedance.

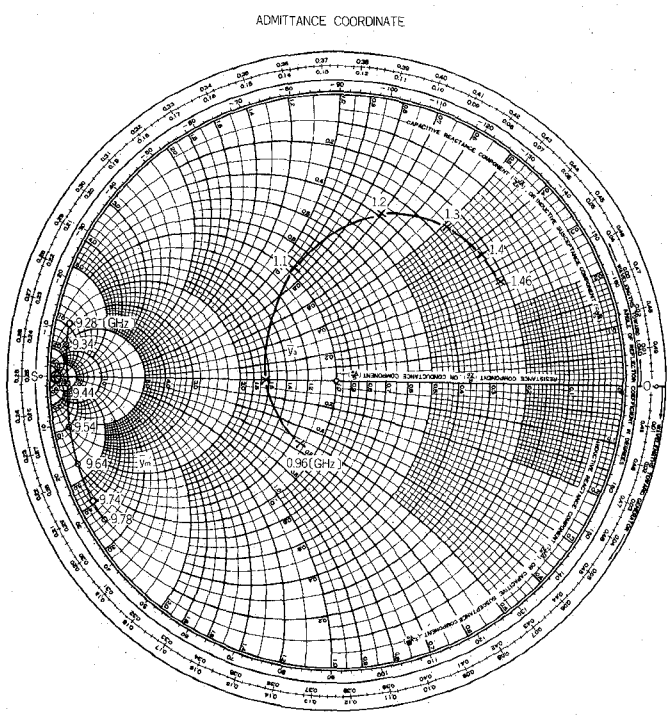

Fig. 9. Frequency performance of normalized input admittance $\bar{y}_a$ of IF amplifier and normalized intrinsic image admittance $\bar{y}'_m$ (normalized by 20 m℧).

B. Input Admittance of IF Amplifier

The frequency performance of the normalized input admittance $\bar{y}_a$ of an IF preamplifier whose first stage is constructed with a field effect transistor is shown in Fig. 9. These measured values are normalized by 20 m℧. The values of VSWR of this amplifier are less than 5.

C. Input and Outward Admittances at Terminal s

In the case where connecting the input admittance y_a of IF preamplifier at the IF port and the given external circuit at the image port as shown in Fig. 2(a), the value of the outward admittance y_{sa} can be calculated by (6). $\bar{y}_{sa}$ signifies the outward admittance normalized by the characteristic admittance of a ridged guide.

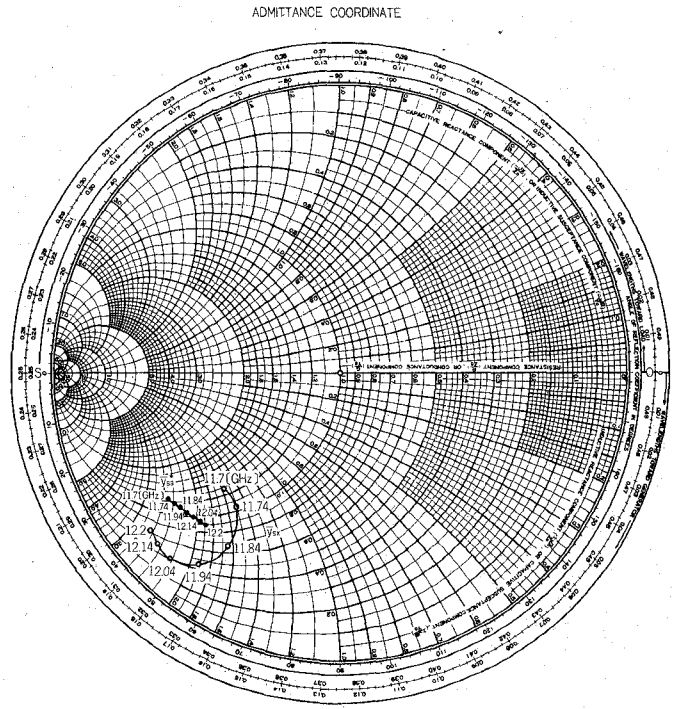

Fig. 10. Normalized input admittance $\bar{y}_{sx}$ and conjugate normalized outward admittance $\bar{y}^*_{sa}$ at terminal s in signal frequency band (normalized by characteristic admittance of ridged guide).

The input admittance y_{sx} at terminal s can be calculated by using (19), (5), and (6)

$$y_{sx} = j\omega_s C_c + 1/\left(R_s + j\omega_s L + \frac{1}{y'_{sx} + j\omega_s C_0} \right). \quad (19)$$

Many circuits parameters in these equations are obtained in Sections IV and VI.

The frequency performance of the normalized input admittance $\bar{y}_{sx}$ of the SHF down converter and the conjugate normalized outward admittance $\bar{y}^*_{sa}$ at terminal s are shown in Fig. 10. $\bar{y}_{sx}$ and $\bar{y}^*_{sa}$ show a rather good match in the signal frequency band (11.7–12.2 GHz).

The values of VSWR at the IF port are less than 5 as shown in Fig. 9, and these values are reduced to less than 2.5 at the signal port, caused by the conversion loss (approximately 3 dB).

D. Noise Figure

The theoretical value of the total noise figure F of the SHF down converter can be obtained using (17). The details of this calculation are explained in Section III-B and the Appendix. The results are shown in the following section.

VI. Frequency Performance of Noise Figure

The theoretical and measured values of the total noise figure of the SHF down converter with IF preamplifier connected are shown in Fig. 11. The measured values of

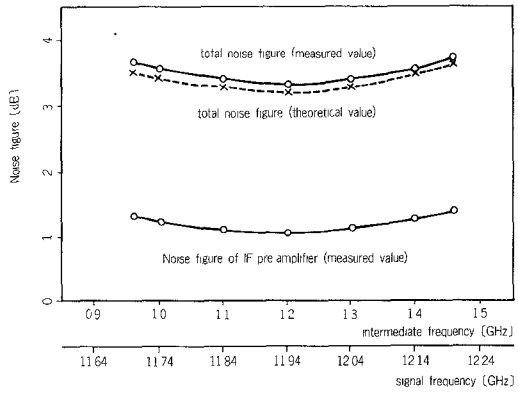

Fig. 11. Noise performance of SHF down converter.

the noise figure of the IF preamplifier are shown in Fig. 11. The calculation is performed by using the following numerical values for the diode's constants in (7), (9), (10), (13), (15), (16), and (17) and Fig. 2: $\alpha = 34.7$, $i_0 = 2\times10^{-13}$ A; $C = 0.07$ pF; $C_c = 0.13$ pF; $V_\phi = 0.8$ V; $R_s = 1.5\ \Omega$; $L = 0.4$ nH; $L_W = 1.8$ nH; $L_s = 7$ nH; and $n_i = 1.1$. It is necessary to use the results shown in Figs. 3–10 for this calculation.

In Fig. 11, the theoretical value of the total noise figure is 3.2–3.6 dB; the experimental value is 3.3–3.7 dB. These results can be regarded as a good agreement and within the margin of observational error of the noise measurement.

VII. Conclusion

The frequency performance of the noise figure of the SHF down converter made by a planar circuit mounted in a waveguide has been obtained. The theoretical and experimental values of this frequency performance were found to agree well. It has also been confirmed that the optimum image impedance is a short circuit if the down converter is to have a wide frequency band and low-noise characteristics.

It has been made clear how mismatching between the down converter and the IF preamplifier affects the noise performance and the input matching condition. Additionally, in order to achieve a smaller value of the total noise figure over a wide frequency band, the value of the input VSWR of the IF preamplifier must be reduced without increasing the value of its noise figure F_{1f}.

For example, assuming the input VSWR of this IF preamplifier decreased less than 2.5 (half of the present value) without deteriorating its noise performance, this present analysis predicts that the total noise figure F would be reduced to 2.7 to 3.1 dB in the same frequency band shown in Fig. 11. Therefore the development of a low-noise IF preamplifer having a low-input VSWR characteristic will become an important subject for research.

And the analysis including the effect of local oscillator harmonics is also an important subject for research. In connection with this, the research will be continued by using the Held and Kerr's theoretical method [11] in the future.

Appendix

Derivation of Noise Temperature Ratio Corresponding to Shot Noise t'_{ac}

In order to analyze the behavior of the shot noise, y'_{s1}, y'_{s1l}, y'_{i1}, y'_{i1l}, y''_{m1}, and y'_{m1} must be obtained.

The values of y'_{s1} and y'_{s1l} with loaded y'_{ia} at terminal i' and with y'_m at terminal m' can be obtained as shown in (A2) by substituting (A1) into (3)

$$I'_i = -y'_{ia}V'_i \qquad I'_m = -y'_mV'_m \tag{A1}$$

$$\begin{aligned}
y'_{s1} &= g_0 + g_pA_{is} + g_{2p}A_{ms}\\
y'_{s2} &= j\omega_s(C_pA_{is} + C_{2p}A_{ms})\\
y'_{s1l} &= y'_{sa} + y'_{s2}\\
A_{is} &= (g_p + j\omega_iC_p)(g_{2p} - g_0 - y'^*_m - j\omega_mC_{2p})/H_1\\
A_{ms} &= \{(g_p + j\omega_iC_p)(g_p - j\omega_mC_p)\\
&\quad -(g_{2p} - j\omega_mC_{2p})(g_0 + y'_{ia})\}/H_1\\
H_1 &= (g_0 + y'_{ia})(g_0 + y'^*_m)\\
&\quad -(g_p - j\omega_mC_p)(g_p + j\omega_iC_p).
\end{aligned} \tag{A2}$$

Similarly, the values of y'_{i1} and y'_{i1l} with loaded y'_{sa} at terminal s' and with y'_m at terminal m', and the values of y''_{m1} and y'_{m1} with loaded y'_{sa} at terminal s' and with y'_{ia} at terminal i' are given as shown in (A3) and (A4)

$$\begin{aligned}
y'_{i1} &= g_0 + g_p(A_{si} + A_{mi})\\
y'_{i2} &= j\omega_iC_p(A_{si} + A_{mi})\\
y'_{i1l} &= y'_{ia} + y'_{i2}\\
A_{si} &= \{(g_p - j\omega_mC_p)(g_{2p} + j\omega_sC_{2p})\\
&\quad -(g_p + j\omega_sC_p)(g_0 + y'^*_m)\}/H_2\\
A_{mi} &= \{(g_p + j\omega_sC_p)(g_{2p} - j\omega_mC_{2p})\\
&\quad -(g_p - j\omega_mC_p)(g_0 + y'_{su})\}/H_2\\
H_2 &= (g_0 + y'_{sa})(g_0 + y'^*_m)\\
&\quad -(g_{2p} - j\omega_mC_{2p})(g_{2p} + j\omega_sC_{2p})
\end{aligned} \tag{A3}$$

$$\begin{aligned}
y''_{m1} &= g_0 + g_pA^*_{im} + g_{2p}A^*_{sm}\\
y'_{m1} &= y'_m + y''_m - y''_{m1}\\
A_{sm} &= \{(g_p + j\omega_iC_p)(g_p + j\omega_sC_p)\\
&\quad -(g_{2p} + j\omega_sC_{2p})(g_0 + y'_{ia})\}/H_3\\
A_{im} &= (g_p + j\omega_iC_p)(g_{2p} - g_0 - y'_{sa} + j\omega_sC_{2p})/H_3\\
H_3 &= (g_0 + y'_{sa})(g_0 + y'_{ia})\\
&\quad -(g_p + j\omega_iC_p)(g_p + j\omega_sC_p).
\end{aligned} \tag{A4}$$

The shot noise currents I_{ni}, I_{ns}, and I_{nm} appearing at terminal i'_1, s'_1, and m'_1 of the g circuit in Fig. 2(b) will then be obtained. The conversion loss L'_{gsi} and L'_{gmi} are given in

(A5):

$$L'_{gsl}=\frac{|Y'_{gsl}|^2}{|y'_{s1}-y'_{gssm}|^2}\cdot\frac{g'_{s1}}{g'_{t1l}}$$

$$L'_{gml}=\frac{|Y'_{gml}|^2}{|y'^{*}_{m1}-Y'_{gmms}|^2}\cdot\frac{g''_{m1}}{g'_{t1l}}$$

$$Y'_{gsl}=Y'_{gls}=g_p-g_pg_{2p}/(g_0+y'^{*}_{m1})$$

$$Y'_{gssm}=g_0-g_{2p}^2/(g_0+y'^{*}_{m1})$$

$$Y'_{gml}=Y'_{glm}=g_p-g_pg_{2p}/(g_0+y'_{s1l})$$

$$Y'_{gmms}=g_0-g_{2p}^2/(g_0+y'_{s1l}). \tag{A5}$$

The mismatching loss $L_{s1,\text{in}}$, $L_{m1,\text{in}}$, and $L_{t1,\text{out}}$ are given in (A6):

$$L_{s1,\text{in}}=\frac{|y'_{s1l}+y'_{s1}|^2}{4g'_{s1l}g'_{s1}}$$

$$L_{m1,\text{in}}=\frac{|y'_{m1}+y''_{m1}|^2}{4g'_{m1}g''_{m1}}$$

$$L_{t1,\text{out}}=\frac{|y'_{1l}+y'_{t1l}|^2}{4g'_{t1}g'_{t1l}}. \tag{A6}$$

The available noise power supplied to g'_{t1l} from y'_{s1l} which is kept in $nkT_0[K]$ $(n=19.5/\alpha)$ [18] is given as $nkT_0/(L_{s1,\text{in}}\cdot L'_{gsl})$. That supplied to g'_{t1l} from y''_{m1} kept in $nkT_0[K]$ is given as $nkT_0/(L_{m1,\text{in}}\cdot L'_{gml})$. The total available noise power supplied to g'_{t1l} from y'_{s1l}, y''_{m1}, and the g circuit itself which is kept in $nkT_0[K]$ is given as $nkT_0/L_{t1,\text{out}}$. Therefore the noise power supplied to g'_{t1l} generated in the g circuit only can be defined as N_t, as shown in (A7) and Fig. 3.

$$N_t=nkT_0B_t$$

$$B_t=\frac{1}{L_{t1,\text{out}}}-\frac{1}{L_{s1,\text{in}}\cdot L'_{gsl}}-\frac{1}{L_{m1,\text{in}}\cdot L'_{gml}}. \tag{A7}$$

The shot noise current I_{nl} is given by (A8) [5],[15]

$$I_{nl}=y'_{t1l}\cdot\sqrt{\frac{N_t}{g'_{t1l}}}. \tag{A8}$$

Similarly, the shot noise current I_{ns} and I_{nm} are shown in (A9) and (A10), respectively

$$I_{ns}=y'_{s1l}\sqrt{\frac{N_s}{g'_{s1l}}}$$

$$N_s=nkT_0B_s$$

$$B_s=\frac{1}{L_{s1,\text{out}}}-\frac{1}{L_{t1,\text{in}}\cdot L'_{gls}}-\frac{1}{L_{m1,\text{in}}\cdot L'_{gms}}$$

$$L'_{gls}=\frac{|Y'_{gls}|^2}{|y'_{t1}-Y'_{glm}|^2}\frac{g'_{t1}}{g'_{s1l}}$$

$$L'_{gms}=\frac{|Y'_{gms}|^2}{|y''^{*}_{m1}-Y'_{gmml}|^2}\cdot\frac{g''_{m1}}{g'_{s1l}}$$

$$L_{t1,\text{in}}=\frac{|y'_{t1l}+y'_{t1}|^2}{4g'_{t1l}\cdot g'_{t1}}$$

$$L_{s1,\text{out}}=\frac{|y'_{s1}+y'_{s1l}|^2}{4g'_{s1}g'_{s1l}}$$

$$Y'_{glm}=g_0-g_p^2/(g_0+y'^{*}_{m1})$$

$$Y'_{gsm}=Y'_{gms}=g_{2p}-g_p^2/(g_0+y'_{t1l})$$

$$Y'_{gmml}=Y'_{gssl}=g_0-g_p^2/(g_0+y'_{t1l}) \tag{A9}$$

$$I_{nm}=y'_{m1}\sqrt{\frac{N_m}{g'_{m1}}}$$

$$N_m=nkT_0B_m$$

$$B_m=\frac{1}{L_{m1,\text{out}}}-\frac{1}{L_{s1,\text{in}}\cdot L'_{gsm}}-\frac{1}{L_{t1,\text{in}}\cdot L'_{glm}}$$

$$L'_{gsm}=\frac{|Y'_{gsm}|^2}{|y'_{s1}-Y'_{gssl}|^2}\cdot\frac{g'_{s1}}{g'_{m1}}$$

$$L'_{glm}=\frac{|Y'_{glm}|^2}{|y'_{t1}-Y'_{glls}|^2}\cdot\frac{g'_{t1}}{g'_{m1}}$$

$$L_{m1,\text{out}}=\frac{|y''_{m1}+y'_{m1}|^2}{4g''_{m1}g'_{m1}}$$

$$Y'_{gls}=g_0-g_p^2/(g_0+y'_{s1l}). \tag{A10}$$

Next it must be considered how I_{nl}, I_{ns}, and I_{nm} reach Re (y'_{ia}) at the IF output terminal i' in Fig. 2(b). Many kinds of current transfer functions α are defined as follows. For example, α_{gsl} is the transfer function from terminal s' to i' of g circuit, and is expressed as (A12) by using (A11).

$$I'_{i1}=Y'_{gls}V'_s+Y'_{glm}V'_t$$

$$I'_{i1}=-y'_{t1l}V'_t \qquad I'_{s1}=y'_{s1}V'_s \tag{A11}$$

$$\alpha_{gsl}=-I'_{i1}/I'_{s1}=-Y'_{gls}y'_{t1l}/\{y'_{s1}(y'_{t1l}+Y'_{glm})\}. \tag{A12}$$

Similarly, $\alpha_{gsm}(=-I'^{*}_{m1}/I'_{s1})$, $\alpha_{gms}(=-I'_{s1}/I'^{*}_{m1})$, $\alpha_{gml}(=-I'_{t1}/I'^{*}_{m1})$, $\alpha_{gls}(=-I'_{s1}/I'_{t1})$, $\alpha_{glm}(=-I'^{*}_{m1}/I'_{t1})$, $\alpha_{csl}(=-I'_{tz}/I'_{s2})$, $\alpha_{csm}(=-I'^{*}_{mz}/I'_{s2})$, $\alpha_{cms}(=-I'_{s2}/I'^{*}_{m2})$, $\alpha_{cml}(=-I'_{t2}/I'^{*}_{m2})$, $\alpha_{cls}(=-I'_{s2}/I'_{t2})$, and $\alpha_{clm}(=-I'^{*}_{m2}/I'_{t2})$ can also be obtained.

Other current transfer functions β are defined as follows. For example, β_{lgc} is that from terminal i'_1 to i'_2, and $\beta_{lgc}=y'_{i2}/y'_{i1l}$. Similarly, $\beta_{sgc}=y'_{s2}/y'_{s1l}$, $\beta_{mgc}=y''_{m2}/y'_{m1}$, $\beta_{lcg}=y'_{i1}/y'_{i2l}$, $\beta_{scg}=y'_{s1}/y'_{s2l}$, and $\beta_{mcg}=y''_{m1}/y'_{m2}$.

And as mentioned in Section III-B, the approximation of $\omega_t\ll\omega_s$, ω_m cannot be used. Therefore all passes shown in Fig. 3 must be considered, as the down-converter action of C circuit can not be neglected.

Using several kinds of α and β, the relation given by

(A13) can be obtained, where I_{ni}, I_{ns}, and I_{nm} are given by (A8)–(A10)

$$\begin{bmatrix} 1 & 0 & 0 & -\beta_{scg}\alpha_{gsi} & 0 & -\beta^*_{mcg}\alpha_{gmi} \\ 0 & 1 & -\beta_{sgc}\alpha_{csi} & 0 & -\beta^*_{mgc}\alpha_{cmi} & 0 \\ 0 & -\beta_{icg}\alpha_{gis} & 1 & 0 & 0 & -\beta^*_{mcg}\alpha_{gms} \\ -\beta_{igc}\alpha_{cis} & 0 & 0 & 1 & -\beta^*_{mgc}\alpha_{cms} & 0 \\ 0 & -\beta_{icg}\alpha_{gim} & 0 & -\beta_{scg}\alpha_{gsm} & 1 & 0 \\ -\beta_{igc}\alpha_{cim} & 0 & -\beta_{sgc}\alpha_{csm} & 0 & 0 & 1 \end{bmatrix} \cdot \begin{bmatrix} I_{i1o} \\ I_{i2o} \\ I_{s1o} \\ I_{s2o} \\ I^*_{m1o} \\ I^*_{m2o} \end{bmatrix} = \begin{bmatrix} I_{ni} \\ 0 \\ I_{ns} \\ 0 \\ I^*_{nm} \\ 0 \end{bmatrix}. \quad \text{(A13)}$$

The total output shot noise current I_{io} appearing at terminal i' can be derived from (A13) as shown in (A14)

$$\begin{aligned} I_{io} &= \frac{g'_{ia}}{y'_{i1l}} I_{i1o} + \frac{g'_{ia}}{y'_{i2l}} I_{i2o} \\ &= g'_{ia}\left[\left(\frac{A_1}{y'_{i1l}} - \frac{A_2}{y'_{i2l}}\right)\cdot I_{ni} + \left(\frac{A_3}{y'_{i1l}} - \frac{A_4}{y'_{i2l}}\right)\cdot I_{ns} \right. \\ &\quad \left. + \left(\frac{A_5}{y'_{i1l}} - \frac{A_6}{y'_{i2l}}\right)\cdot I^*_{nm}\right]. \end{aligned} \quad \text{(A14)}$$

In (A14), $A_1 - A_6$ are functions of several kinds of current transfer functions α and β, and can be calculated from (A13) and (A14). I_{ni}, I_{ns}, and I_{nm} are not coherent with one another. Therefore the shot noise power supplied to g'_i at terminal i' can be expressed by the sum of the values computed separately.

Therefore t'_{ac} is obtained by (15), and then t and F are given by (16) and (17).

ACKNOWLEDGMENT

The author wishes to thank Dr. Y. Konishi, the Director for Research at the NHK Technical Research Laboratories for his guidance and many helpful discussions.

REFERENCES

[1] Y. Konishi, K. Uenakada, N. Yazawa, N. Hoshino, and T. Takahashi, "Simplified 12-GHz low-noise converter with mounted planar circuit in waveguide," *IEEE Trans. Microwave Theory Tech.*, vol. MTT-22, pp. 451–454, Apr. 1974.

[2] Y. Konishi, *The Design of SHF Receiver for Broadcasting*, Sanpo, 1974.

[3] Y. Konishi, Y. Utsumi, and N. Hoshino, "SHF low noise receiver for satellite broadcasting," in 1976 Nat. Conv. Rec. Inst. Electron. Commun. Eng. Japan, Optic and Electromagnetic Wave Division, No. 150.

[4] Y. Konishi, "12 GHz band FM receiver for satellite broadcasting," presented at IEEE Electron. Aerospace Syst. Conv., 19-4-EASCON 77, Sept. 1977.

[5] Y. Konishi, "12 GHz band FM receiver for satellite broadcasting," *IEEE Trans. Microwave Theory Tech.*, vol. MTT-26, pp. 720–725, Oct. 1978.

[6] H. C. Torrey and C. A. Whitmer, *Crystal Rectifiers*, MTT Radiation Lab. Series, vol. 15. New York: McGraw-Hill, 1948.

[7] E. W. Herold, R. R. Bush, and W. R. Ferris, "Conversion loss of diode mixers having image-frequency impedance," *Proc. IRE*, vol. 33, pp. 603–609, Sept. 1945.

[8] P. D. Strum, "Some aspects of crystal mixer performance," *Proc. IRE*, vol. 41, pp. 875–889, July 1953.

[9] M. R. Barber, "Noise figure and conversion loss of the Schottky barrier mixer diode," *IEEE Trans. Microwave Theory Tech.*, vol. MTT-15, pp. 629–635, Nov. 1967.

[10] C. S. Kim, "Tunnel-diode converter analysis," *IRE Trans. Electron Devices*, vol. ED-8, pp. 394–405, Sept. 1961.

[11] D. N. Held and A. R. Kerr, "Conversion loss and noise of microwave and millimeter-wave mixers: Part 1—Theory," *IEEE Trans. Microwave Theory Tech.*, vol. MTT-26, pp. 49–55, Feb. 1978.

[12] D. N. Held and A. R. Kerr, "Conversion loss and noise of microwave and millimeter-wave mixers: Part 2—Experiment," *IEEE Trans. Microwave Theory Tech.*, vol. MTT-26, pp. 55–61, Feb. 1978.

[13] Y. Utsumi and Y. Konishi, "Analysis of image recovery down converter," in 1977 Nat. Conv. Rec. Inst. Electron. Commun. Eng. Japan, no. 680.

[14] Y. Utsumi and Y. Konishi, "Frequency performance of image recovery down converter," in 1979 Nat. Conv. Rec. Inst. Electron. Commun. Eng. Japan, no. 730.

[15] Y. Utsumi and Y. Konishi, "Analysis of image recovery down converter," *Journal Inst. Television Eng. Japan*, vol. 33, no. 3, pp. 216–221, Mar. 1979.

[16] Y. Utsumi and Y. Konishi, "Frequency performance of image recovery down converter," in 1981 Nat. Conv. Rec. Inst. Electron. Commun. Eng. Japan, no. 764.

[17] Y. Konishi, "Planar circuit mounted in waveguide used as a down converter," *IEEE Trans. Microwave Theory Tech.*, vol. MTT-26, pp. 716–719, Oct. 1978.

[18] G. L. Ragan, *Microwave Transmission Circuits*. New York: McGraw Hill, p. 108.

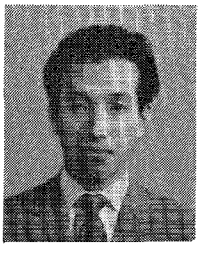

Yozo Utsumi (M'81) was born in Osaka, Japan, on August 3, 1943. He received the B. Eng. and the M. Eng. degrees from Osaka University (Osaka Daigaku), Osaka, Japan, in 1966, and 1968, respectively.

He joined Nippon Hoso Kyokai (Japan Broadcasting Corporation), Tokyo, in 1968. Since 1971 he has worked at their Technical Research Laboratories, where he has been engaged in research and development of VHF, UHF, and Microwave circuits, and has been involved in the analysis and design of the low noise receiver for satellite broadcasting.

Mr. Utsumi is a member of IECEJ (Institute of Electrical Communication Engineering of Japan) and ITEJ (Institute of Television Engineering of Japan).